Nonlinear dynamic conversion of analog signals into excitation patterns

Gerold Baier* and Markus Müller
Facultad de Ciencias, Universidad Autonoma del Estado de Morelos, 62210 Cuernavaca, Morelos, Mexico
(Received 30 August 2003; revised manuscript received 14 May 2004; published 29 September 2004)

Local periodic perturbations induce frequency-dependent propagation waves in an excitable spatiotemporally chaotic system. We show how segments of noise-contaminated and chaotic perturbations induce characteristic sequences of excitations in the model system. Using a set of "tuned" excitable systems, it is possible to characterize signals by their spectral composition of excitation pattern. As an example, we analyze an epileptic "spike-and-wave" time series.

DOI: 10.1103/PhysRevE.70.037201 PACS number(s): 05.45.Gg, 05.45.Tp, 05.45.Xt

For systems of diffusively coupled nonlinear oscillators, it was found that excitable spatiotemporal chaos may undergo a generic pattern transition when perturbed locally at an appropriate frequency [1]. The switching from a globally disordered pattern of low mean amplitude to a globally ordered pattern of traveling excitation waves can be used for the "detection" of the perturbation frequency. To do this, one can simply record the induced excitations, i.e., the suprathreshold firing of one of the model's elements.

A related detection principle is exploited in the time series analysis performed by the ear (see e.g., Ref. [2]). In the mammalian inner ear, for example, sound-induced mechanical vibrations are converted into sequences of nerve cell firings that propagate as excitation waves to the auditory cortex. There, the temporal patterns of excitations are interpreted with high accuracy and noise tolerance, in spite of the original sound signal's complexity and nonstationarity. The common assumption in the modeling of this process is that the spikes are induced from a resting state that is an excitable fixed point [3]. However, it was shown recently that both spontaneous and induced neural excitation patterns can be modeled with a resting state that is low-dimensional chaos [4]. Furthermore, it was shown that this might even *improve* the reliability of induced firing.

We have suggested that the pattern transition reported in Ref. [1] be used as a device to analyze time series that are noise contaminated and nonstationary [5]. So far, the following problems have not been dealt with: (i) How does the response of such a system depend on perturbation amplitude and frequency; (ii) how does the system react in the presence of noise in the signal; (iii) what is the temporal resolution, and (iv) how is the response to experimental signals. Here, we study these questions using a prototypic model system.

The model is a set of nonlinear excitable oscillators coupled by (linear) diffusion in one spatial dimension in the following form:

$$\frac{1}{\varepsilon}\frac{dX_1}{dt} = f(X_1,Y_1) + D_X(X_2 - X_1) + \mathcal{P}/(A\varepsilon),$$

$$\frac{1}{\varepsilon}\frac{dY_1}{dt} = g(X_1,Y_1),$$

$$\frac{1}{\varepsilon}\frac{dX_i}{dt} = f(X_i,Y_i) + D_X(X_{i+1} + X_{i-1} - 2X_i),$$

$$\frac{1}{\varepsilon}\frac{dY_i}{dt} = g(X_i,Y_i), \tag{1}$$

$$\frac{1}{\varepsilon}\frac{dX_N}{dt} = f(X_N,Y_N) + D_X(X_{N-1} - X_N),$$

$$\frac{1}{\varepsilon}\frac{dY_N}{dt} = g(X_N,Y_N),$$

for $i=2,3,\ldots,N-1$, where N, the number of oscillators, is chosen to be 30, and the boundary conditions are zero flux. Parameter ε is a velocity constant that is identical for all variables of the unperturbed differential equation. For a given external perturbation, the model velocity (and thereby the model's internal frequencies) can be adjusted by changes in ε. The additive term $\mathcal{P}$ (not affected by changes of ε) denotes the local external perturbation. Its strength is controlled by coupling parameter A. The nonlinear functions f and g are adapted from the Goldbeter–Dupont–Berridge model [6]:

$$f(X,Y) = a - m_2X/(1+X) + m_3YX^2/((k_1+Y)(k_a+X^2)) + Y - X,$$

$$g(X,Y) = m_2X/(1+X) - m_3YX^2/((k_1+Y)(k_a+X^2)) - Y.$$

In the absence of external perturbation, the chain of oscillators has spatiotemporally hyperchaotic solutions [1]. With model parameters fixed in the Canard region of the individual oscillator, [7] the chaos is *excitable*, i.e., a single short perturbation exceeding some threshold value leads to a spike of significantly larger amplitude than the spontaneous oscillations (see Ref. [8]). However, in spite of being an excitable medium, the exponential divergence of the basal chaos prevents any long-range propagation of waves following a single local suprathreshold perturbation.

If a sinusoidal periodic perturbation is added to the equation for variable X_1 of the first oscillator, $\mathcal{P}=\sin(\omega t)$, with amplitude $1/A$, excitation waves can be induced for some frequency windows of the perturbation [1]. These large-

*Electronic address: baier@servm.fc.uaem.mx

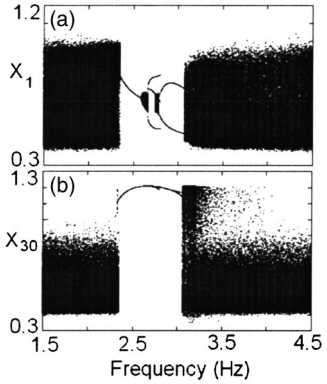

FIG. 1. Bifurcation diagram of Eq. (1) with additive sinusoidal forcing of X_1 in the form $\mathcal{P}=\sin(\omega t)$. Plotted are maxima of variables X_1 (a) and X_{30} (b) as a function of forcing frequency ω. Parameters: $a=0.325$, $m_2=20$, $m_3=23$, $k_1=0.8$, $k_a=0.81$, $\varepsilon=1.0$, $D_X=0.5$, and $A=80$.

amplitude waves propagate from the point of perturbation to the far end of the chain. Figure 1 is a bifurcation diagram showing maxima of variables X_1 and X_{30} as a function of forcing frequency ω. In Fig. 1(a), the two dark regions in the plot of X_1 ($1.5<\omega<2.3$, and $3.1<\omega<4.5$) indicate perturbed (hyper-)chaotic behavior with a distribution of maxima that is wider than in the chaotic resting state. In contrast, the central region ($2.3<\omega<3.1$) indicates periodic or quasiperiodic behavior of medium amplitude. It is in this window that excitation waves are generated. In Fig. 4(b), the left dark region and the far right region in the plot of X_{30} ($1.5<\omega<2.3$ and $4.0<\omega<4.5$, respectively) are due to chaotic behavior with a distribution of maxima that is equal to the chaotic resting state. In these bands, the influence of the perturbation is much weaker than in Fig. 1(a). The region $3.1<\omega<4.0$ is a mixture of basal chaos and irregularly induced excitation waves. The central region ($2.3<\omega<3.1$) of Fig. 1(b) is formed by periodic oscillations of large amplitude. In this window, the induced large-amplitude excitation waves reach the far end of the chain of oscillators. The periodic window maintains its size in the frequency domain throughout the chain. The small region of complex bifurcations within the periodic window in the center of Fig. 1(a) is lost in the course of propagation. From oscillator 16 onward, the bifurcation structure remains qualitatively unchanged. This shows how the spatiotemporal arrangement of excitable units acts as a kind of sharp-edged band-pass filter.

For $A>95$, no excitation waves are detected in oscillator 30, i.e., a minimum coupling strength is required to start the process of propagation. For $80<A<95$, the frequency window of induced excitations widens as coupling strength is increased. For $40<A<80$, the frequency window remains nearly constant in width. In addition, for stronger couplings, new windows with more complex excitation waves, like periods 2 and 3, appear.

The periodic excitation waves do not stabilize an unstable periodic orbit of the unperturbed system [1]. Therefore, the induced excitation waves do not follow an orbit of the unperturbed system and are not an example of successful chaos control by external periodic forcing as introduced by Pyragas [9].

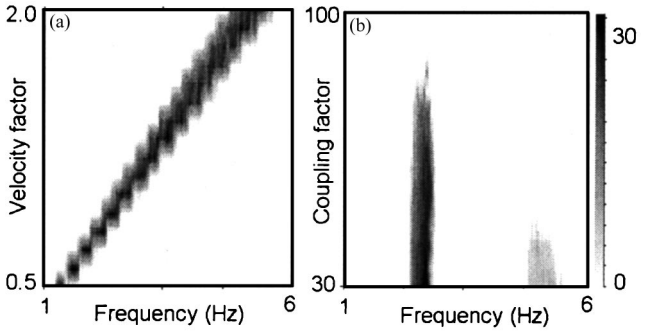

FIG. 2. Scans in parameter space of Eq. (1) with $\mathcal{P}=\sin(\omega t)+\eta$, where η denotes white noise (zero mean; variance 1). Grey coding of number of suprathreshold maxima in variable X_{30} in response to 30 sine wave cycles in the perturbation. Average of 30 runs for each point. (a) Parameter plane ε/ω; $A=40$. (b) Parameter plane A/ω; $\varepsilon=1.0$. Other parameters as in Fig. 1.

The Fourier spectrum of the unperturbed chaos in Eq. (1) has a broadband distribution with well-pronounced maxima at about 3.4 and 3.6 s^{-1}. The frequency range for which induction of excitation waves is found does not coincide with these maximum power frequencies. If Eq. (1) is scanned with a coupling of the sine wave for which no periodic excitation waves are induced at all, the mean amplitude of the response does not increase in the range $2.3<\omega<3.1$. If Fourier spectra are calculated for this case, we observe a clear maximum of the power in the frequency range where excitation waves are induced for stronger couplings. This power maximum is a consequence of the prolonged fraction of time that the system spends near the "ghost" of the periodic solution and thus indicative of the nearby crisis. The results thus differ from classical resonant firing as seen, e.g., in the periodically forced Hodgkin–Huxley equation [10].

Analysis of the bifurcations that lead to excitation waves shows that at both $\omega\approx2.3$ and $\omega\approx3.1$, the chaotic attractor undergoes a crisis. If the perturbation frequency is chosen within the excitation window and initial conditions are selected on the unperturbed chaotic attractor, chaotic transients are observed that follow trajectories similar to the unperturbed case for some time. Within this frequency region, a chaotic attractor that closely resembles the attractor seen, e.g., at $\omega=2.2$, can be stabilized if the unperturbed chaotic signal is used as external driving. The mechanism that locally suppresses the chaos thus requires that the periodic forcing destabilizes the chaotic solution in a crisis and turns it into a chaotic saddle.

Now we study the dependence of the induction of excitation waves in the presence of noise in the perturbation. The chosen perturbation consists of Gaussian white noise (mean zero and amplitude variance equal to 1) to which a sequence of 30 full cycles of the sine wave of amplitude 1 is added. Figure 2 shows scans of two parameter planes for Eq. (1) with this perturbation. In order to obtain results that are independent of the particular choice of initial conditions, the average of 30 runs with different initial conditions is evaluated for each set of parameters. This way, the effect of randomly induced excitation waves [especially near the high-frequency end of the periodic window in Fig. 1(b)] is

suppressed. Successful induction is characterized by the number of induced excitation waves exceeding a threshold value in oscillator 30. The threshold is set as 0.7 of variable X_{30} (a value that is not exceeded in the averaged chaotic basal state).

In the ω-ε-plane [Fig. 2(a)], a single band is found where excitation waves are induced whereas the rest shows no excitation at all. The band is displaced linearly and widens slightly as the frequency is increased. The relationship between velocity factor and perturbation frequency at maximum induction is given in linear regression as $\varepsilon = 2.6\omega$. The horizontal width of the band allows an estimation of the frequency resolution. The resolution is better than in the case of a pure sine wave (Fig. 1) because the noise tends to impede the induction of excitation waves and this effect is stronger near the borders of the induction band. Furthermore, the results in Fig. 2(a) are averages over 30 runs with different initial condition. This averaging is essential to improve the frequency resolution compared to Fig. 1(b). The chaotic excitations adjacent to the region of regular excitation are thereby suppressed. Figure 2(b) shows the scan of parameter plane A-ω at fixed ε. Here, parameter A controls the amplitude of the combined noise and sine-wave perturbation and does not affect the relative amplitude of the two contributions. In Fig. 2(b), the dark tongue centered at $\omega \approx 2.8$ Hz represents a unique induction zone for couplings $A > 40$. For stronger couplings ($A < 40$), the structure gets more complex as harmonics of the optimal perturbation frequency also succeed in inducing waves. The first harmonic is visible as a light gray zone at $\omega \approx 5.6$. At even lower values of A, new bifurcations lead to more complex types of excitation waves, e.g., period 2 and period 3 solutions as in the case of pure sinusoidal perturbation (see Ref. [11]).

The unperturbed system is not a classical excitable medium. Its basal state is spatiotemporally chaotic, i.e., it displays an irregular temporal evolution in all variables. We perturbed Eq. (1) with the combined sine-wave-white noise signal as in Fig. 2 and calculated how long it takes (averaged over 30 runs) for the first induced excitation wave to reach oscillator 30 after the onset of the sine wave. Figure 3(a) shows that the average propagation time depends on forcing frequency like $1/\omega$. By plotting the result in terms of number of sine-wave cycles in the perturbation, a constant of 11–12 cycles is found. On the average, this number of perturbation cycles in oscillator 1 are completed before the first excitation wave reaches oscillator 30. (The resulting time delay Δt is used to shift the time axes for each frequency in Fig. 4, accordingly.)

The frequency-resolved response of subthreshold spatiotemporal chaos to transient irregular perturbations has not been studied previously. Because of the noise tolerance (Fig. 1) and the temporal resolution (Fig. 2), it should be possible to characterize the main frequencies as well as continuous changes of the main frequencies in such signals. To study such a case, we chose an epileptic oscillation as recorded by a scalp electroencephalogram (EEG). This type of nonharmonic oscillation has been analyzed with respect to its complexity and it was concluded that it presents an example of a low-dimensional chaotic process [12,13]. For the analysis, the EEG signal was normalized (average zero, variance equal

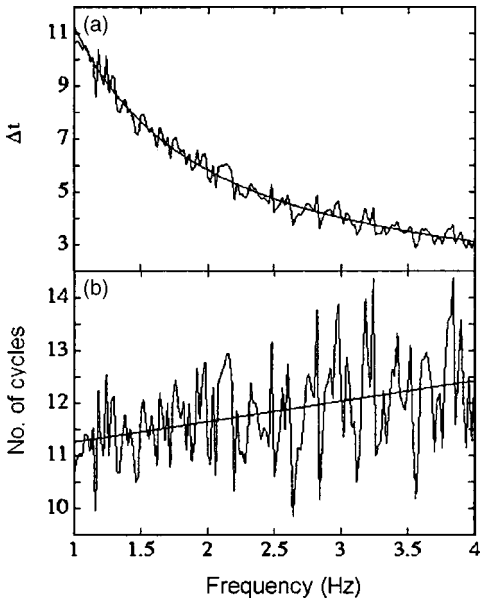

FIG. 3. Mean response time of variable X_{30} to the onset of perturbation in variable X_1 as a function of ω; (a) expressed in seconds; and (b) expressed as number of perturbation cycles. For each perturbation frequency ω, parameter ε is calculated as $\varepsilon = \omega/2.6$ according to the calibration in Fig. 2. Plotted are averages of 30 runs at each point. Other parameters as in Fig. 1.

to 1, using an episode free of artifacts and seizure activity as a reference). During the epileptic event, there is a sudden rearrangement of the frequency composition from the broadband "normal" electric activity to a comparatively regular sequence of so-called spike-and-wave complexes [Fig. 4(a)]. The Fourier spectrum of this section shows a dominant frequency on a basal broadband distribution as is typical for this type of seizures [12].

The coupling is chosen such that the broadband normal EEG signal does not induce any excitation waves. This way the normal activity is ignored and only the seizure activity

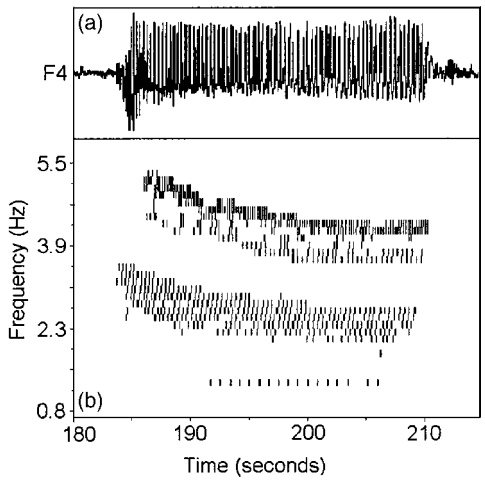

FIG. 4. (a) EEG signal (electrode F4) with epileptic activity. The seizure lasts from 183–211 s. (b) Excitations of a set of Eq. (1) with different parameters ε perturbed by the EEG signal in (a). Plot as in Fig. 4. $A = 120$, other parameters as in Fig. 1.

with its dominant frequencies and large amplitudes is detected. Figure 4(b) is the pattern of induced waves during the time where the seizure occurs in the signal. The pattern displays three bands. The two main bands are centered initially at 3.4 Hz and 5.0 Hz, respectively. The frequency band at about 3 Hz corresponds to the dominant frequency of the spike-and-wave complexes. Clearly, the higher-frequency band is not a harmonic of the lower-frequency band but a second independent frequency. Both bands undergo a shift in frequency to final values of 2.6 Hz and 4.4 Hz, respectively. This reflects the well-documented frequency slowing during absence seizures [14]. The thin third band at about 1.4 Hz starts approximately at second 192 and lasts until second 207. It is a subharmonic of the main frequency, which in this part of the seizure is centered at 2.8 Hz. Thus, while the fine texture of the two broadbands does not permit to distinguish between a noisy limit cycle and deterministic chaos, the appearance of a subharmonic indicates a degree of complexity typical of a chaotic attractor.

The system Eq. (1) in its "tuned" form exploits the properties of spatiotemporal excitable chaos to extract information from analog signals and represent them as temporally evolving excitation patterns. Some of its features are: (1) A minimum number of recurrent excitations are required to be detectable. This successfully suppresses uncorrelated noise components in the signal. (2) The sharp-edged filter characteristic (Fig. 2) permits induction of waves only in a certain frequency band. This allows a separation of contributions with distinct frequencies in the signal and estimation of their individual frequencies even in the presence of high levels of noise. (3) Onset, offset, and continuous shifts in frequency of the band are features that allow almost instantaneous detection and characterization of *transient* events (see Fig. 4). (4) In contrast to Fourier spectra, wavelets, and methods derived from nonlinear dynamics (e.g., the estimation of the correlation dimension or of the spectrum of Lyapunov characteristic exponents) no predetermined finite window of data (with assumed stationarity) is required for evaluation. The system identifies "interesting" episodes in nonstationary recordings. Its temporal resolution makes the method attractive for the analysis of time series where nonstationarity is not only unavoidable but also crucial for the understanding, e.g., EEG recordings or, in the context mentioned in the introduction, the sound-generated vibrations in the inner ear. (5) Finally, the combination of data normalization with a preset value of coupling constant allows *automatic* detection and characterization of specific events (e.g., sounds with characteristic overtones and undertones [2]).

The fact that the unperturbed system is excitable allows one to not only detect events and changes of events in the perturbation but also—as soon as they disappear—to automatically destroy the induced coherence and to reset the basal dynamics. The method thus differs from nonresetting artificial neural networks and has dynamics closer to those of sensory neurons which are supposed to give "*a sort of running commentary*" [3] to an external signal's temporal variations. This recommends the present system for further investigation with respect to information extraction.

This work was supported by CONACyT, Mexico (Project No. 40885-F). The authors thank U. Stephani and H. Muhle, Clinic for Neuropediatry, University of Kiel, Germany, for providing the data set used in Fig. 4.

[1] G. Baier, S. Sahle, J. P. Chen, and A. Hoff, J. Chem. Phys. **110**, 3251 (1999).
[2] W. L. Gulick, G. A. Geschieder, and R. D. Frisina, *Hearing—Physiological Acoustics, Neural Coding, and Psychoacoustics* (Oxford University Press, New York, 1989).
[3] F. Rieke, D. Warland, R. de Ruyter van Stevenick, and W. Bialek, *Spikes—Exploring the Neural Code* (MIT Press, Cambridge, MA, 1998).
[4] G. Baier, G. J. Escalera, H. Perales, M. Rivera, M. Müller, R. Leder, and P. Parmananda, Phys. Rev. E **62**, R7579 (2000).
[5] G. Baier, R. Leder, and P. Parmananda, Phys. Rev. Lett. **84**, 4501 (2000).
[6] A. Goldbeter, G. Dupont, and M. Berridge, Proc. Natl. Acad. Sci. U.S.A. **87**, 1461 (1990).
[7] P. Strasser, O. E. Rössler, and G. Baier, J. Chem. Phys. **104**, 9974 (1996).
[8] G. Baier, M. Müller, and H. Ørsnes, J. Phys. Chem. B **106**, 3274 (2002).
[9] K. Pyragas, Phys. Lett. A **170**, 421 (1992).
[10] P. Parmananda, C. Mena, and G. Baier, Phys. Rev. E **66**, 047202 (2002).
[11] P. Parmananda, S. Sahle, and G. Baier, Z. Phys. Chem. (Munich) **216**, 499 (2002).
[12] A. Babloyantz and A. Destexhe, Proc. Natl. Acad. Sci. U.S.A. **83**, 3513 (1986).
[13] R. Friedrich and C. Uhl, Physica D **98**, 171 (1996).
[14] E. Niedermeyer, in *Electroencephalography*, edited by E. Niedermeyer and F. Lopes da Silva, 4th Ed. (Lippincott Williams & Wilkins, Philadelphia, 1999), p. 476.